Insight Into the Role of Polymers in the Bulk Synthesis of MgF 2 for the Fluorination of 2-Chloropyridine

Julien Dieu, Francesca François, Anne Sophie Mamede, Isabelle Batonneau-Gener, Sagrario Pascual, Vincent Maisonneuve, Amandine Guiet, Sylvette Brunet

ChemCatChem

Research Article
doi.org/10.1002/cctc.202501064

Chemistry Europe
European Chemical Societies Publishing

www.chemcatchem.org

Insight Into the Role of Polymers in the Bulk Synthesis of MgF_2 for the Fluorination of 2-Chloropyridine

Julien Dieu,[a] Francesca François,[b] Anne Sophie Mamede,[c] Isabelle Batonneau Gener,[a] Sagrario Pascual,[b] Vincent Maisonneuve,[b] Amandine Guiet,[b] and Sylvette Brunet*[a]

MgF_2 is one of the most active catalysts for the Cl/F exchange in the transformation of 2-chloropyridine. This study presents a more environmentally friendly and straightforward method for preparing bulk MgF_2 nanoparticles (NP) in aqueous solution. The presence of a structuring agent such as PMMA or Pluronic F68 as polymers, leads to a higher specific surface area after HF treatment (around 30%). It contributed to its preservation under hydrogen fluoride, reflecting the operating conditions for the fluorination of 2-chloropyridine. Regarding the catalytic activity, no change was observed for NP MgF_2 synthesized in water with or without microwave heating. In contrast, an increase (around 20%) in activity for the transformation of 2-chloropyridine was noted when a polymer was used during the preparation correlating with an increase of the specific surface area.

1. Introduction

Fluorinated molecules have become indispensable in the chemical industry due to their exceptional physicochemical properties, such as lipophilicity, dipole moment, pKa, and reactivity.[1,2] Fluorine is present in more than 25% of pharmaceutical products and 40% of agrochemical products, making it a key element in organic synthesis.[3–5] Over the past few decades, numerous fluorinated building blocks containing one or more fluorine atoms or groups (e.g.,—CF_3 and —CHF_2) have been developed for the synthesis of increasingly sophisticated molecules, contributing to the global increase of the agrochemical market.[6,7] The high global demand for innovation in Li-ion battery technology has further driven manufacturers to develop advanced systems using fluorinated compounds as electrolytic additives.[7–9] However, fluorinated organic compounds are rarely found in their natural state, necessitating the development of efficient synthetic methods. From an fluor atom-economy perspective, hydrogen fluoride (HF) is an ideal candidate, accounting for 95% of the reagent's weight. Currently, the catalyzed fluorination of chlorinated molecules is limited to industrial applications involving nonfunctionalized aliphatic molecules, producing chlorofluoroalkanes (CFCs), hydrofluorocarbons (HFCs), and, more recently, hydrofluoroolefins (HFOs) due to their negative impact of CFCs on the ozone layer and HFCs in greenhouse effect.[10] There is no industrial catalytic process for the synthesis of fluorinated aromatic or functionalized fluorinated aliphatic compounds. In the case of aromatics, production relies on multi-step organic syntheses, such as the Halex reaction or the Balz–Schiemann reaction. These methods are poorly selective and generate substantial saline waste, posing significant environmental challenges.[11–14] Previous studies[15–18] have demonstrated the feasibility of a catalyzed fluorination reaction using 2-chloropyridine as a model molecule. This reaction involves a selective Cl/F exchange to produce 2-fluoropyridine and HCl as a recyclable by-product. Such a method avoids carbon loss and eliminates saline waste, making it environmentally friendly and process-efficient. Optimal reaction conditions include a temperature of 350 °C, an excess of HF (HF/2-chloropyridine molar ratio = 11), and a catalyst based on bulk magnesium fluoride (MgF_2) prepared using trifluoroacetic acid and magnesium acetate as precursors.[16] However, the catalyst's specific surface area remains low (35 m^2/g) due to the thermal treatment at 450 °C required to remove the majority of carbon deposits from the catalyst surface. The specific surface area is a critical parameter for enhancing catalytic activity, as it increases the number and the accessibility of active sites. Optimizing the preparation method and the synthesis parameters of the catalyst is therefore crucial to improve its performances.

Several so-called "soft chemistry" methods are used to prepare metal fluorides with significant specific surface areas, such as sol–gel synthesis[19–26] and microwave-assisted synthesis.[27,28] From the sol–gel synthesis, various metal fluorides with high specific surface areas, often X-ray amorphous, have been pre-

[a] J. Dieu, I. B. Gener, S. Brunet
Institut de Chimie des Milieux et Matériaux de Poitiers (IC2MP), UMR 7285 CNRS, Université de Poitiers, 4 rue Michel Brunet TSA 71106- 86073 Poitiers Cedex 9, France
E-mail: sylvette.brunet@univ-poitiers.fr

[b] F. François, S. Pascual, V. Maisonneuve, A. Guiet
Institut des Molécules et Matériaux du Mans (IMMM), UMR 6283 CNRS, Le Mans Université, Avenue Olivier Messiaen 72085 Le Mans Cedex 9, France

[c] A. S. Mamede
Unité de Catalyse et de Chimie du Solide (UCCS) UMR CNRS 8181, Université de Lille, Cité Scientifique, Villeneuve d'Ascq Cedex 59655, France

pared, such as AlF_3 (100–500 m^2 g^{-1}),[19–21] MgF_2 (150–350 m^2 g^{-1}),[22–24] ZnF_2 (140 m^2 g^{-1}).[25] Alternatives have therefore been proposed, in which alkoxide precursors are replaced by metal salts such as nitrates, carboxylates, or halides.[25] Moreover, the textural properties of these materials, and in particular their specific surface area, are highly sensitive to the calcination temperature. The specific surface area decreases markedly with temperature, as metal fluorides generally crystallize between 200 and 500 °C. For example, the specific surface area of MgF_2, which is 350 m^2 g^{-1} at room is reduced to only 29 $m^2.g^{-1}$ after thermal treatment at 350 °C in air.[23–24] The treatment of bulk MgO (initial specific surface area of ~300 m^2/g) with HF yields pure bulk MgF_2 but reduces the specific surface area to ~35 $m^2.g^{-1}$.[15] Similarly, solvothermal methods using microwaves as a heat source and various magnesium precursors (nitrate, acetate, chloride, or carbonate), with or without a structuring agent (e.g., polymethyl methacrylate, PMMA beads), do not prevent the loss of the specific surface area in the operating reaction conditions, leading to similar catalytic activity (~30 mmol $h^{-1}g^{-1}$). Notably, when PMMA is used as a structuring agent, the catalytic activity is even lower than 30 mmol $h^{-1}g^{-1}$).[17,18]

This study aims to investigate the influence of different synthesis parameters on the structural and physicochemical properties of MgF_2 nanoparticles (NPs), prepared either by room-temperature precipitation or by solvothermal synthesis using microwave heating. Specifically, the effects of i) the solvent (methanol or water), ii) the use of microwaves (MW) as a heat source, and iii) the presence of a polymer as structuring agent such as PMMA latex or a commercial Pluronic (F68) during the MgF_2 synthesis are investigated. These two polymers were initially chosen because they are commonly used to disperse metal oxide nanoparticles. It was therefore of interest to extend their use to metal fluorides.[29,30] All MgF_2 samples were characterized, and their performance was evaluated for the transformation of 2-chloropyridine.

2. Experimental Section

2.1. Catalyst Preparations and Chemicals

2.1.1. Polymer-Free Synthesis of Bulk MgF_2 Nanoparticles (NP)[17]

Chemical reagents used for the synthesis of polymer-free bulk MgF_2 catalyst were as follows: Magnesium carbonate hydroxide ($Mg_5(CO_3)_4(OH)_2.4H_2O$, Acros Organics); Hydrofluoric acid solution ($HF_{40\%}$, 27.6 mol·L^{-1}) and methanol (by Sigma-Aldrich).

Bulk MgF_2 NP were synthesized by a precipitation method using magnesium carbonate as the precursor and aqueous hydrofluoric acid ($HF_{40\%}$) as the fluorinating agent (Scheme 1). Two main parameters were investigated: the nature of the solvent (water or methanol) and the reaction temperature, either room temperature or 90 °C using microwave heating. In a typical synthesis, 1.8743 g of magnesium carbonate was introduced into a Teflon chamber reactor. 14 mL of the selected solvent (methanol or water) were added under stirring, followed by the addition of 1.74 mL of aqueous hydrofluoric acid ($HF_{40\%}$) corresponding to a F/Mg molar ratio of 2. For the reaction at 90 °C under microwave heating, the reactor was inserted into a MARS-6 Microwave Digestion System (CEM Corp.) equipped with temperature and pressure sensors. The temperature was ramped up to 90 °C within 5 min and maintained for 30 min. For reaction at room temperature, the same procedure was followed without heating. In both cases, the resulting gel-like product was collected, washed three times with ethanol by centrifugation, and dried in an oven at 80 °C. The synthesis yielded a white MgF_2 nano-powder. Samples were named according to the solvent used and the reaction temperature. Those prepared at 90 °C under microwave (MW) heating were labelled MgF_2_MW_methanol and MgF_2_MW_water, while those prepared at room temperature were named MgF_2_methanol and MgF_2_water.

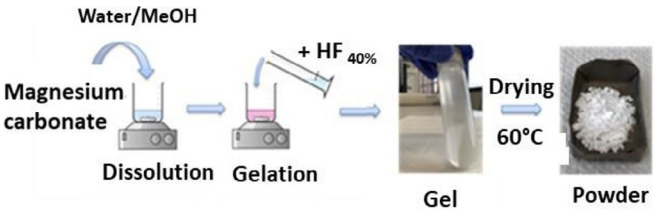

Scheme 1. Synthesis of MgF_2 NP.

2.1.2. Preparation of Bulk MgF_2 Nanoparticles with Polymer Addition[18]

The polymers used were Pluronic F68 (Poly (ethylene glycol)-*block*-poly (propylene glycol)-*block*-poly(ethylene glycol), PEG-PPG-PEG, M_n = 8400 g/mol, Sigma-Aldrich) and home-made PMMA (poly(methyl methacrylate)) beads (Figure 1).

As reported previously, for the home-made PMMA beads the chemicals used were as followed: methyl methacrylate (MMA, ≥ 99%, stabilized, Sigma-Aldrich), ammonium persulfate (APS, 98%, Merck), aluminum oxide (activated, neutral, Brockmann I), were used. MMA was passed through a column of aluminum oxide prior to polymerization. Ultrapure water was obtained from a PureLab ELGA system and had a resistivity of 18.2 MΩ cm^{-1} at 25 °C.

Typically, the procedure began by adding 0.2 g of ammonium persulfate as an initiator, 20 mL of acetone, and 60 mL of ultrapure water into a three-neck flask serving as the reaction medium. The flask was equipped with a reflux condenser and placed in an ice bath. While the mixture was homogenized using a magnetic stirrer, nitrogen gas was purged into the reaction medium, which was maintained in an ice-bath. After 30 min, 1 mL of previously degassed MMA was added to the mixture. The temperature was then increased to 70 °C, and the reaction was allowed to proceed for 4 h under nitrogen. Finally, the reaction medium was cooled to room temperature, and the resulting white polymer latex was used without further purification. The hydrodynamic diameter (D_h) and polydispersity index (PDI) of the resulting polymer template were measured by Dynamic Light Scattering (DLS), yielding D_h = 206 nm and PDI = 0.02.

(a) *Preparation of bulk MgF_2 in the presence of polymers*

MgF_2 NP were synthesized at room temperature in water as described above.[18]

As depicted in Scheme 2, the methodology to target MgF_2 mesoporous materials comprises four steps: (step 1) syntheses of the two buildings blocks (fluoride NP and polymer template) and their dispersion as an homogenous aqueous colloidal mixture, (step 2) fluoride NP/polymer template assembly process via solvent evaporation to obtain the MgF_2 composite, (step 3) calcination including concomitant polymer removal and inorganic fluorinated network densification, (step 4) final thermal treatment under F_2 to remove carbon residue.

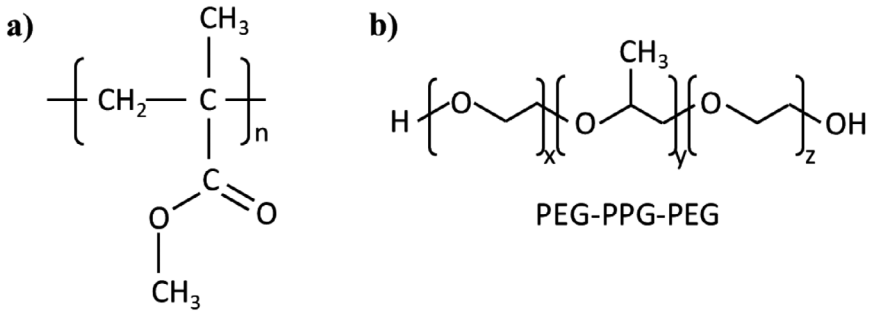

Figure 1. Chemical structure of polymers. a) PMMA b) Pluronic F68.

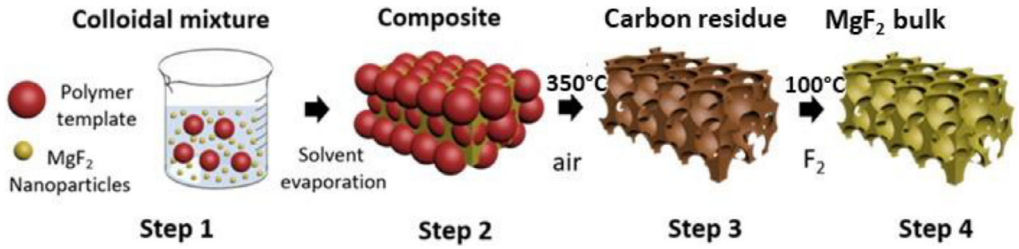

Scheme 2. Synthesis of MgF_2 in the presence of polymer as structuring agent.[18]

More precisely, in their gel form, the MgF_2 NP were dispersed in 75 mL of an acidic aqueous solution (HCl) by stirring for 2 h to obtain an homogeneous colloidal solution (step 1). The polymer (Pluronic F68 as powder or home-made PMMA beads as latex) was subsequently added with a polymer/MgF_2 mass ratio of 2.

After 1 h of stirring, the mixture was then poured into several Teflon plates with a diameter of 25 cm and dried in an oven at 120 °C for 15 h (step 2). The polymers were thermally decomposed in air at 350 °C for 2 h (step 3), followed by a treatment with fluorine gas (F_2) at 100 °C for 1 h to minimize carbon residues (step 4). The calcination under F_2 gas was carried out in a specific equipment dedicated to molecular fluorine, automatically controlled in order to guarantee constant experimental conditions. The catalysts compound was spread evenly in a passivated nickel boat that was introduced in a nickel reactor surrounded by a classic horizontal split furnace. The samples were then dehydrated at 140 °C under dynamic primary vacuum followed by filling of the reactor with nitrogen. The temperature was set to $T = 100$ °C and a mixture of 10% F_2 in nitrogen (Air Liquide) was flowed through the reactor under dynamic conditions for 2 h before being flushed by nitrogen.

MgF_2 prepared by this method was designated as MgF_2_water_PMMA when PMMA was used as the polymer template, and as MgF_2_water_F68 when F68 was used as the polymer template. Table 1 provides a summary of the nomenclature for the different MgF_2 samples based on the operating conditions.

Table 1. MgF_2 sample nomenclature depending on the operating conditions.

Samples	Heating source	Solvent	Polymer
MgF_2_MW_water	MW	water	No
MgF_2_MW_methanol	MW	methanol	No
MgF_2_water	No	water	No
MgF_2_methanol	No	methanol	No
MgF_2_water_PMMA	No	water	PMMA
MgF_2_water_F68	No	water	F68

MW = microwave;PMMA: polymethyl methacrylate; F68: commercial Pluronic F68.

2.2. Characterizations

2.2.1. N_2 Sorption

Specific surface areas were measured at 77 K using a TriStar II 3020 (Micromeritics). The powders were degassed under secondary vacuum at 100 °C for 12 h prior to measurement. The S_{BET} was calculated using the Brunauer – Emmett – Teller (BET) method. The pore size distribution was evaluated from adsorption branches of the N_2 isotherms using the BJH model. The total pore volume was estimated from the nitrogen adsorbed amount at the relative pressure $P/P_0 = 0.99$.

2.2.2. X-Ray Diffraction

The diffractograms were recorded, using an Empyrean diffractometer (PANalytical) equipped with a copper anode. The anode is bombarded with an electron beam generated by a 45 kV voltage and a 40 mA current, producing X-rays. The resulting beam is filtered to isolate the copper Kα_1 and Kα_2 lines ($\lambda K\alpha_1 = 1.54{,}056$ Å, $\lambda K\alpha_2 = 1.544{,}390$ Å). These monochromatic x-rays are then directed onto the sample, and the diffracted x-rays are recorded using a linear detector with an acquisition window set to 2°. All diffractograms were recorded over a 2θ angular range from 15° to 85°, with a step size of 0.033°. The counting time at each step was fixed at 240 s. Samples were prepared on a silica sample holder, which was covered with a Kapton window for air-sensitive samples. Peak identification was carried out using the HighScorePlus software (PANalytical©) and the ICDD database.

2.2.3. FTIR CO Spectroscopy

As described previously,[15] CO adsorption was followed by FTIR on a ThermoNicolet NEXUS 5700 spectrometer with a resolution of 2 cm^{-1} and 64 scans per spectrum. Samples were pressed into thin pellets (10—60 mg) with a diameter of 16 mm and pre-treated in situ during one night under nitrogen at 300 °C. After that, the cell was cooled down with liquid nitrogen to 100 K. A background spectrum was collected which was then subtracted from the following spectra obtained after CO adsorption. Then, successive doses of CO were introduced quantitatively, and an infrared spectrum was recorded after each adsorption until saturation. The final spectrum was recorded with 1 Torr of CO at equilibrium pressure (saturation). All spectra were normalized to an equivalent sample mass (25 mg). The quantification of the amount of Lewis acid sites Qs (µmol g^{-1}) was carried out by the integration of the total area of the IR bands at saturation between 2100 and 2200 cm^{-1} using the molar absorption coefficient ε determined for MgF_2 and equal to 1.53 µmol cm^{-1}.

2.2.4. XPS

The analyses were carried out using a Kratos Analytical Axis Ultra DLD spectrometer using a monochromatic Al Kα source (1486.6 eV). The pass energy is 40 eV for an analysis surface of 700 µm × 300 µm. The binding energies were referenced to that of adventitious C 1s at 285.0 eV. Data processing was carried out using CasaXPS software.

2.3. Activation and Catalytic Measurements

As described previously,[15–18] the activation step by HF (Rapid Gaz, France) and the catalytic activity of the various MgF_2 samples for the transformation of 2-chloropyridine (2ClPy) (Sigma-Aldrich) were carried out in a fixed-bed reactor in gas phase. These different MgF_2 samples were diluted with 6 cm^3 of Lonza graphite (size grains between 125 and 200 µm). The catalyst was activated in situ by HF under nitrogen (HF/N_2 molar ratio: 1/4) for 1 h at 350 °C (activation step). Then, 2-chloropyridine was introduced into the reactor using a syringe pump. The partial pressures of the various components were 0.806 bar for HF, 0.075 bar for 2-chloropyridine, and 0.132 bar for nitrogen (HF/2ClPy/N_2: 10.8/1/1.7). The organic gas products were trapped into 1,2-dichloroethane (Sigma Aldrich). HF and HCl were quenched in an aqueous solution of potassium hydroxide at the outlet of the reactor. The organic components were analysed with a Scion 456 gas-phase chromatograph (Bruker) equipped with a DB5 capillary column (inside diameter: 0.2 mm, thickness of the film: 1 µm, and length: 30 m). The oven temperature was increased from 100 to 200 °C at a rate of 5 °C min^{-1}. The catalyst performances were compared at iso-conversion of 2-chloropyridine lower than 25% in order to be in a differential regime. In all cases, only 2-fluoropyridine (2FPy) was observed as the reaction product and HCl as the by-product.

Thus, the selectivity toward 2FPy was equal to 100% and the conversion of 2-chloropyridine corresponded to the 2FPy yield. In these experiments, the molar balance was always higher than 90%. No thermal decomposition of 2-chloropyridine was observed. The catalytic activity A (mmol h^{-1} g^{-1}) was defined as the conversion of 2-chloropyridine multiplied by the flow of 2-chloropyridine (mol h^{-1}) and divided by the mass of the catalyst. The intrinsic catalytic activity Ai (mmol h^{-1} m^{-2}) was calculated taking into account the specific surface area of the catalyst after the activation step by HF. The TOF (h^{-1}) (Turn Over Frequency) was calculated from the catalytic activity (A in mmol h^{-1} g^{-1}) divided by the number of actives sites defined as coordinatively unsaturated metallic sites (Qs in µmol g^{-1}) measured by CO adsorption followed by IR.

3. Results and Discussion

3.1. Synthesis of MgF_2 Nanoparticles (NP)

MgF_2 NP were synthesized by precipitation with magnesium carbonate and aqueous HF (stoichiometric ratio) as the fluorinating agent. The effect of the temperature by using a microwave heating (RT or 90 °C), a solvent (methanol or water), and a structuring agent addition such as PMMA latex beads or Pluronic F68, (Poly(ethylene glycol)-*block*-poly(propylene glycol)-*block*-poly(ethylene glycol), PEG-PPG-PEG) were investigated.

3.1.1. Influence of the Solvent and of Microwaves as Heating Source

XRD analysis confirms that MgF_2 with a rutile-type structure is obtained directly after synthesis (Figure 2a, regardless of the solvent used (water or methanol) or the synthesis temperature (room temperature or 90 °C under microwave heating). Moreover, all samples retain the rutile structure after subsequent treatment with gaseous HF (Figure 2b). The crystallite size ($D \approx 5$ nm), calculated from XRD patterns, are similar across all samples, regardless of the solvent used or whether microwave heating was applied (Table 2). However, after thermal treatment under nitrogen at 350 °C, the crystallite size increases uniformly for all samples to approximately 12–13 nm. A slight increase is observed after HF activation at 350 °C, reaching around 17 nm.

Sample prepared with methanol as solvent, before HF activation (Figure 3a), exhibit type IIb isotherms with H3 hysteresis loop typical of nonrigid aggregates.[31] The high nitrogen adsorbed amounts for high relative pressure correspond to the filling of the intergranular voids. TEM analysis confirms the presence of MgF_2 aggregates, as illustrated by TEM images shown in Figures 4A and 4B. When water is used as solvent (MgF_2_water), the textural properties evolve. On the corresponding isotherm, a clear inflexion point around P/P_0 value equals to 0.85 as well as a decrease of the isotherm slope indicating the end of mesopore filling. Then for higher relative pressures, high nitrogen adsorbed amounts are related to large intergranular void filling. Thus, the nitrogen isotherm for MgF_2_water sample is a mix of type IVb and IIb with a complex hysteresis loop resulting from the dual porosity level. The mesopore distribution shown on Figure 5 is centered at around 6 nm. These small mesopores can be also seen on TEM images (Figure 4Aa) and mostly resulted from the formation of rigid aggregates. TEM analysis shows aggregates of small platelet-shaped crystallites. The size of these aggregates is approximately 20 nm. The mesopores are likely located within the aggregates, while the macro-porosity corresponds to the space between these aggregates. The use of microwave heating during nanoparticle synthesis also deeply impacts MgF_2 textural properties. For example, the MgF_2_MW_water prepared under microwave heating exhibits a type IVb isotherm with a H2 type hysteresis loop, indicating the development of a complex parti-

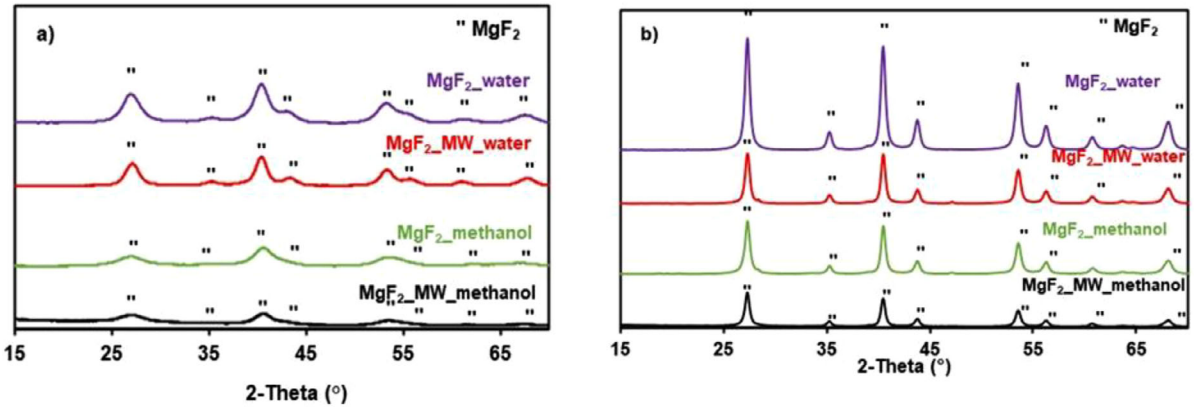

Figure 2. X-ray diffraction diagrams of MgF_2 samples prepared using methanol or water as solvent, with or without microwave heating (MW) during synthesis, a) without treatment and b) after HF activation step.

Table 2. Specific surface area (S_{BET}), cristallite size (D) determined by XRD depending on the operating conditions without thermal treatment, after nitrogen flow at 350 °C during 1 h (After N_2), after HF treatment (HF/N_2 molar ratio = 4) at 350 °C during 1 h (After HF).

Samples	Without treatment		After N_2		After HF	
	S_{BET} (m^2 g^{-1})	D (nm)	S_{BET} (m^2 g^{-1})	D (nm)	S_{BET} (m^2 g^{-1})	D (nm)
MgF_2_MW_methanol	327	4	–	–	49	19
MgF_2_methanol	176	4	43	12	39	16
MgF_2_MW_water	156	7	47	14	41	17
MgF_2_water	151	5	49	13	47	16
MgF_2_water_PMMA	80	12	92	15	80	17
MgF_2_water_F68	112	11	92	18	69	17

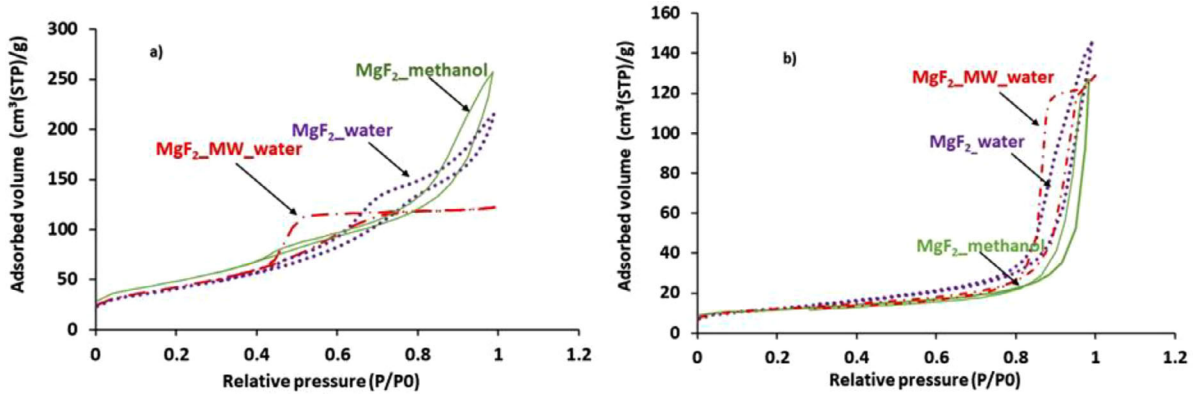

Figure 3. N_2 adsorption–desorption isotherms of MgF_2 samples a) before and b) after the HF activation step.

cle interconnected meso-porosity (Figure 3a). Microwave heating seem to promote the formation of larger nanoparticles and very small and uniform mesopores with a diameter around 5 nm certainly resulting from rigid aggregate formation (Figure 5a). After thermal treatment under HF, the shapes of the nitrogen isotherms and hysteresis loops evolve and become more uniform for all the samples (Figure 5b). The adsorbed nitrogen amounts become significantly lower and the capillary condensation in intergranular voids is delayed to higher relative pressures for all the samples. The corresponding specific surface areas are decreased whereas the particle sizes are increased. These results indicates that HF activation leads to particle growth and modifies NP aggregation state. For example, the samples prepared with and without MW using water as solvent still exhibit a low intergranular meso-porosity with a wide pore size distribution (Figure 5b).

As shown in Table 2, the largest specific surface area (327 $m^2 \cdot g^{-1}$) is observed for MgF_2 nanoparticles prepared using microwave heating (MW) and methanol as the solvent. This value decreases to approximately 170 $m^2 \cdot g^{-1}$ when the synthesis is without MW, value similar to those of syntheses with water. The larger specific surface area of MgF_2 NP observed

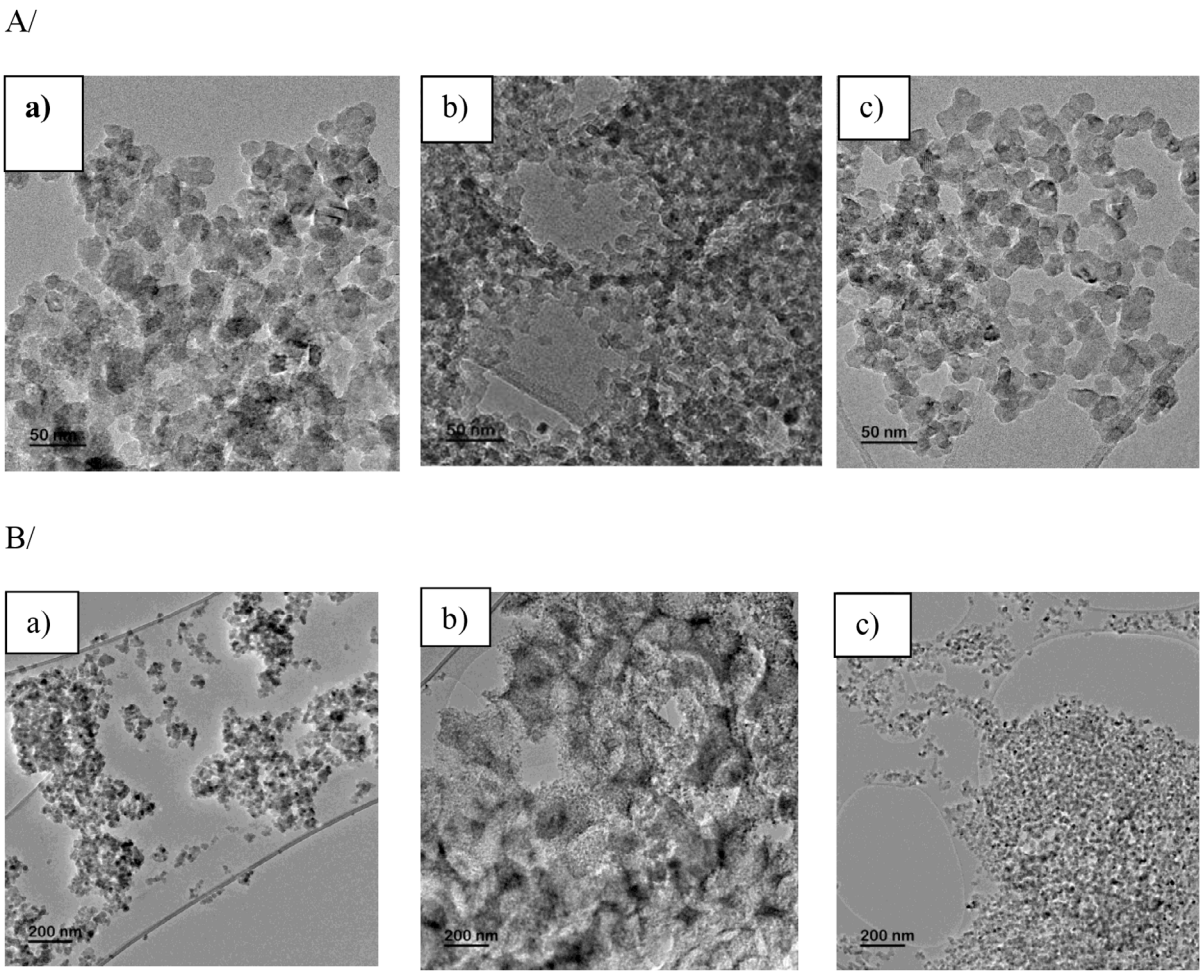

Figure 4. TEM images after the activation step by HF of a) MgF_2_water, b) MgF_2_water_PMMA, and c) MgF_2_water_F68 at two magnifications A/ 50 nm and B/200 nm.

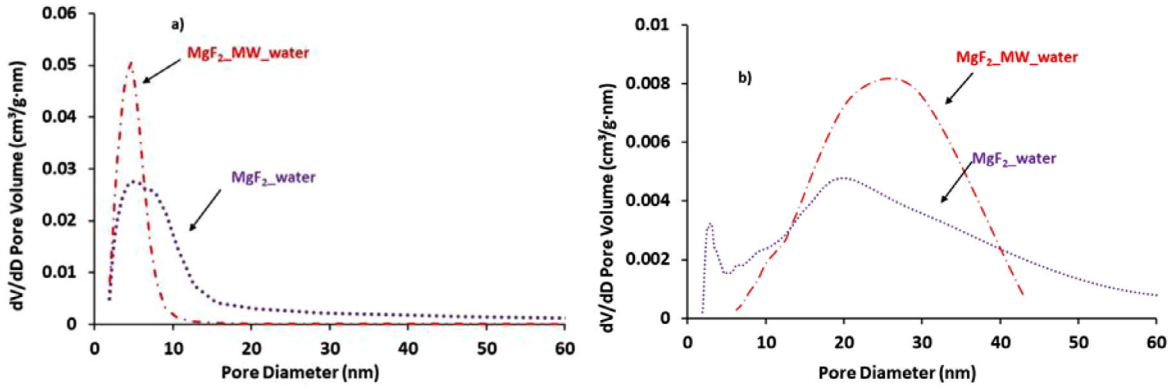

Figure 5. Pore size distributions of MgF_2_water samples obtained with and without MW heating a) before the HF activation step b) after the HF activation step.

for the sample prepared by microwave heating in the presence of methanol is probably related to its lower boiling point compared to water as well as its dielectric parameters, which favor rapid microwave absorption and ultrafast heating. This promotes nucleation at the expense of crystal growth, resulting in smaller particle sizes and higher surface areas. A similar phenomenon has previously been reported in a study investigating the impact of solvent choice on the synthesis of nanosized AlF_3.[32]

Regardless of the initial preparation method, the specific surface areas of all samples prepared without the addition of polymer decrease sharply after treatment under nitrogen at 350 °C, converging to a similar value close to 45 $m^2 \cdot g^{-1}$. After the HF activation step at 350 °C, these specific surface areas remain

Table 3. Specific surface area (S_{BET}), mesopore size (*dp*) depending on the operating conditions without treatment and after HF treatment (HF/N_2 molar ratio = 4) at 350 °C during 1 h (After HF).

Samples	Without treatment		After HF	
	S_{BET} (m^2 g^{-1})	*dp* (nm)	S_{BET} (m^2 g^{-1})	*dp* (nm)
MgF_2_MW_methanol	327	6	49	18–28
MgF_2_methanol	176	3	49	30
MgF_2_MW_water	156	5	41	20–30
MgF_2_water	151	6	47	15–25
MgF_2_water_PMMA	80	9	80	10
MgF_2_water_F68	112	25	69	30

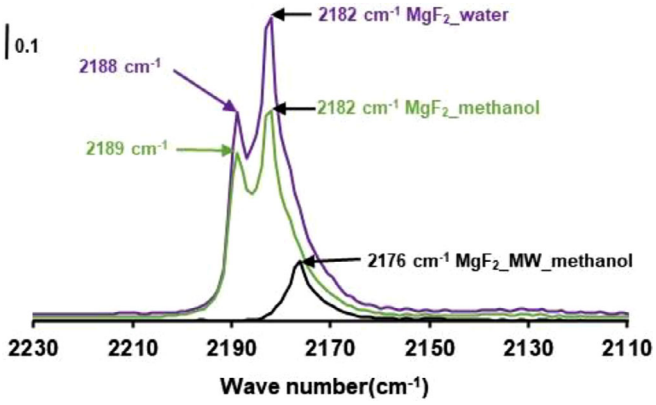

Figure 6. CO adsorption infrared spectra (FTIR-CO): Comparison of MgF_2 prepared using methanol or water as solvent and with or without microwave heating (MW) after activation step by HF (350 °C, 1 h, N_2).

equivalent, stable, and close to the value measured for MgF_2 prepared via the TFA route (using magnesium trifluoroacetate as a precursor), which serves as a reference (≈ 40 $m^2 \cdot g^{-1}$).[16] This decrease highlights the importance of material stability at 350 °C, the operating temperature for the catalytic reaction. The increase of the crystallite size after activation step impacting the particle aggregation certainly explains the decrease of surface area for activated samples (Table 2).

Thus, after N_2 treatment (350 °C, 1 h) and HF activation (T = 350 °C, HF/N_2 = 4/1), the decrease of all specific surface areas can be attributed to the low synthesis temperature (90 °C) of MgF_2 compared to the treatment temperature (350 °C) under HF and N_2, as well as the decomposition of the precursor. Based on these results, the use of microwave heating appears unnecessary, as it does not improve the stability of the surface area after treatment at 350 °C under N_2 or HF. Moreover, water can be used as a safer alternative to toxic solvents such as methanol, when possible. These results suggest that the synthesis process can be simplified to make it more environmentally friendly.

The catalytic properties of active sites (unsaturated coordinating magnesium atoms) involved in the fluorination reaction of 2-chloropyridine as a model molecule were characterized by CO adsorption followed by infrared spectroscopy (FTIR-CO). This technique assessed both the Lewis acidity strength and the active site amount (Figure 6 and Table 4).[16,17]

Initially, the sample MgF_2_MW_methanol (prepared with methanol as the solvent and microwave heating) exhibited a lower Lewis acidity strength than MgF_2 prepared via the TFA route,[16] with a single CO adsorption band at 2177 cm^{-1} compared to 2181 and 2190 cm^{-1} for MgF_2_TFA.[16] Replacing methanol with water as the solvent and/or omitting microwave heating resulted in an increase of the Lewis acidity strength, as evidenced by the shift to two bands at 2182 and 2189 cm^{-1}, corresponding to the values for MgF_2_TFA.

Regarding the quantity of active sites, it was greater for samples prepared without microwave heating (Table 3). No significant influence of the solvent was observed, as the quantity of sites remained around 470 $\mu mol \cdot g^{-1}$ for both MgF_2_methanol and MgF_2_water. Consequently, the concentration of sites per square meter increased to become comparable to those of MgF_2_TFA (≈ 10 $\mu mol \cdot m^{-2}$).

The difference between MgF_2_MW_methanol and the other samples (MgF_2_methanol and MgF_2_water) cannot be explained by differences in specific surface area (which are similar) or NP size. This suggests that MgF_2 particles exist as NP aggregates with varying facet stabilities, as suggested by a theoretical approach.[33]

3.1.2. Influence of the Presence of a Structuring Agent During the Synthesis of Bulk MgF_2

Regardless of the presence or the chemical nature of polymer used during synthesis, the structure of MgF_2 determined by XRD consistently corresponds to the rutile (-ICSD-20513) type both before and after the HF activation step (Figure 7). The MgF_2 NP obtained in the presence of a polymer during the synthesis has a larger diameter than those synthesized without (around 11 nm). According to the TEM images, the particle size appears to be more uniform when a polymer is added (Figure 4A/b, 4B/b) and (Figure 4/c, 4B/c). The chemical nature of the polymer has no influence on particle size. However, nitrogen physisorption results on Figures 8 and 9 and Table 2, suggest that the addition of a polymer during the MgF_2 synthesis deeply impact sample textural properties (Figure 8).

Initially, synthesis without polymer addition and in aqueous solution, MgF_2 (MgF_2_water) has a specific surface area of 151 $m^2.g^{-1}$ (Table 2). In the presence of a polymer, the specific surface areas of the untreated samples is lower (PMMA: 80 m^2 g^{-1}, F68: 112 m^2 g^{-1}). After HF activation at 350 °C, the specific surface areas remain stable at around 90 m^2 g^{-1}, in contrast to MgF_2 prepared without polymer, whose specific surface areas decrease to around 50 m^2 g^{-1}. The nitrogen adsorption-desorption isotherms are very different for the three MgF_2 materials before (Figure 8a) and after the HF activation step (Figure 8b) and illustrate how polymer chemical nature impact MgF_2 particles aggregation. MgF_2_water_F68 exhibits a type IIb isotherms with H3 hysteresis loop typical of nonrigid aggregates (Figure 8a). This result is illustrated on TEM images which show small and uniform aggregated nanoparticles with a size around 11 nm (Figure 4). MgF_2_water and MgF_2_water_PMMA isotherm are very similar (type IVb + II) even through the nitrogen adsorbed amounts are significantly lower when PMMA is used. The use of PMMA also

Table 4. Quantity (μmol.g^{-1}) and concentration (μmol.m^{-2}) of sites determined by FTIR-CO: Comparison of MgF_2 prepared with methanol or water as solvent and with or without microwave heating (MW) after activation by HF (350 °C, 1 h, N_2) (relative uncertainty: 10%).

Sample	Wavenumber (cm^{-1})	Q_{sites} (μmol g^{-1})	S_{BET} (m^2 g^{-1})	C_{sites} (μmol m^{-2})
MgF_2_MW_methanol	2177	87	49	1.7
MgF_2_ methanol	2182	414	39	–
	2189	72		–
	Total	486		12.4
MgF_2_water	2182	415	47	–
	2188	50		–
	Total	465		9.9
MgF_2_water_PMMA	2130	16	80	–
	2180	17		–
	2187	382		–
	Total	415		5.2
MgF_2_water_F68	2182	477	69	–
	2189	53		–
	Total	530		7.7

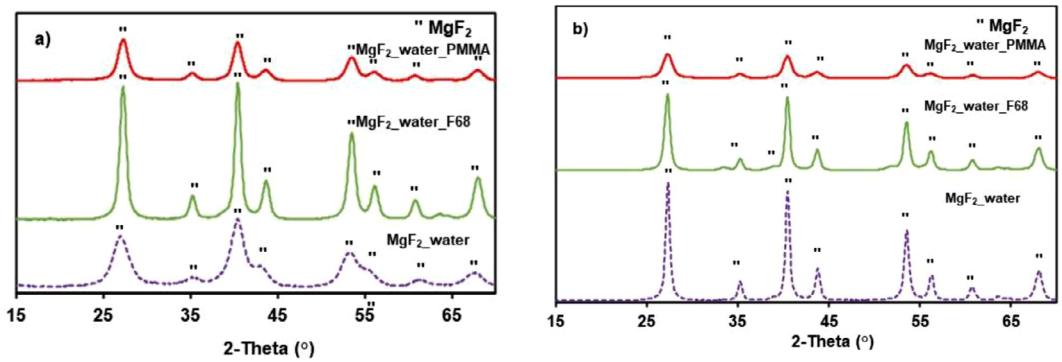

Figure 7. X-ray diffractograms of MgF_2 samples prepared without or with addition of F68 or PMMA a) before and b) after HF activation step.

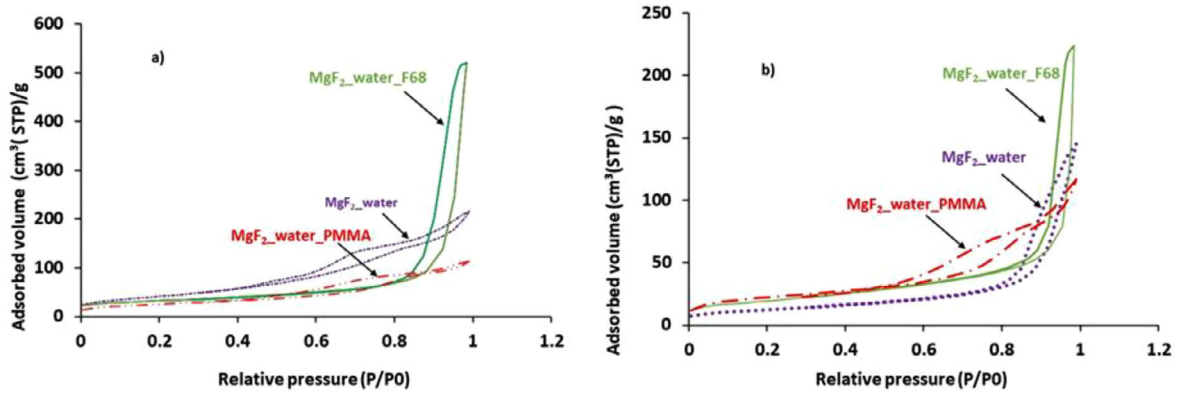

Figure 8. N_2 adsorption and desorption isotherms of MgF_2_water, MgF_2_water_F68, MgF_2_water_PMMA a) before and b) after HF activation step (b).

creates aggregates with dual intergranular porosity. The intergranular mesopore size distribution for MgF_2_water_PMMA is rather large and centered on 9 nm, slightly higher than for its water counterpart (Figure 9a).

After HF activation, the BET specific surface area of the samples synthesized with PMMA or F68 decreases to a lesser extent compared to the MgF_2_water sample, and their specific surface areas remain higher (Table 3). These limited decreases are ascribed to a limited particle size increase after HF activation treatment. When PMMA is used, HF activation has a very low impact on the isotherm shape and the intergranular mesopores are preserved (Figures 8b and 9b). As expected

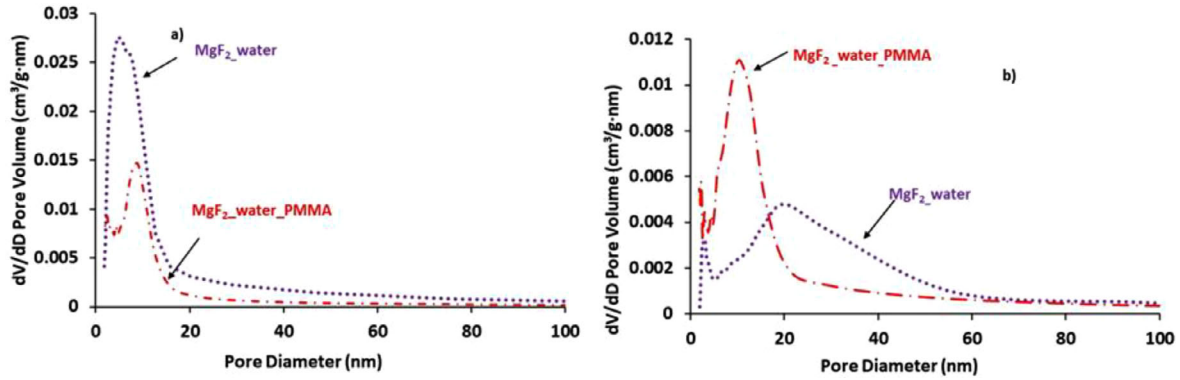

Figure 9. Pore size distributions of MgF_2 a) before and b) after HF activation step.

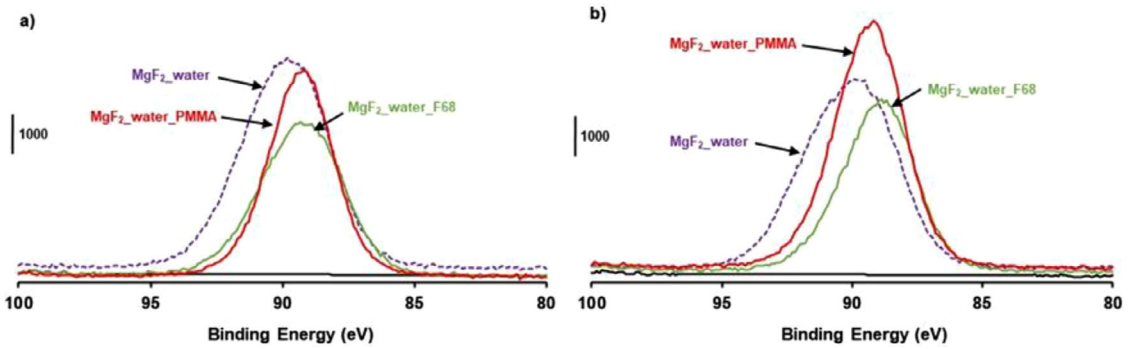

Figure 10. XPS spectra of the Mg 2s regions for MgF_2 prepared without polymer addition and with F68 or PMMA, a) before and b) after HF activation step.

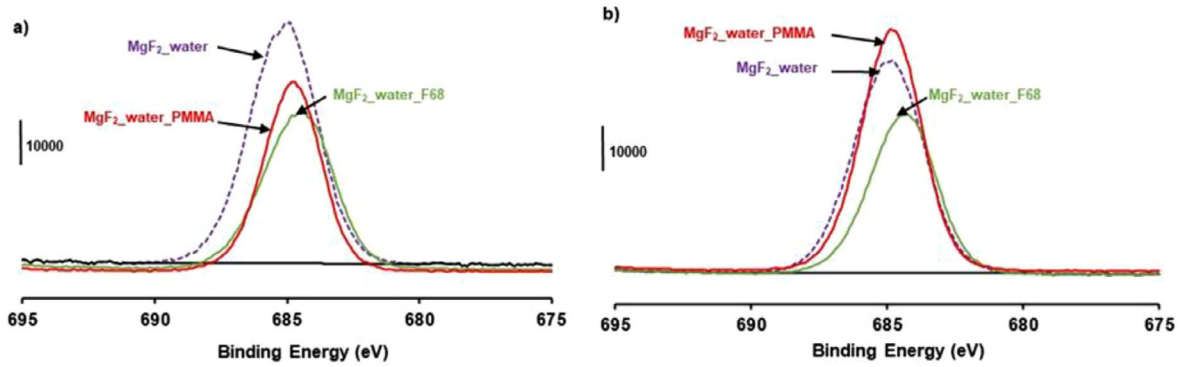

Figure 11. XPS spectra of the F 1s regions for MgF_2 prepared without polymer addition and with F68 or PMMA, a) before and b) after HF activation step.

from textural characterization, particle agglomeration is certainly linked to the polymer chemical-physical properties. The polymer certainly allows a better particle dispersion due to its tensio-active properties. This protective effect leads to NP less agglomerated.

Analysis of the different species on the catalyst surface of these materials by XPS (surface technique) did not reveal any difference related to the addition of F68 or PMMA during the MgF_2 synthesis compared to that without polymer. Spectra of the Mg 2 s (90 eV) (Figure 10), F 1s (684 eV) (Figure 11) and C 1s (283 eV) (Figure 12) regions show similar binding energies with or without polymer addition and this irrespective of the polymer used (F68 or PMMA), and before and after HF activation. Magnesium (≈ 20%) and fluorine (≈ 50%) are the major elements with a Mg/F atomic ratio of around 0.41 corresponding to a MgF_2 structure (Table 5).

The strength in terms of Lewis acidity and the quantification of sites determined by CO adsorption followed by infrared (FTIR-CO) for MgF_2 prepared with F68 or PMMA as polymer is similar to the material without polymer (Figure 13).

They show a similar medium/low strength to MgF_2 prepared by the TFA route (2181 and 2190 cm^{-1}), and a quantity of sites (PMMA: 415 µmol g^{-1}, F68: 530 µmol g^{-1}) similar to the material without polymer (465 µmol g^{-1}) and greater than MgF_2 prepared by the TFA route (270 µmol g^{-1}) after HF activation. In this case, whatever the polymer (PMMA or F68), the concentration of sites remains similar to those of materials prepared without polymer addition and MgF_2 prepared by the TFA route (Table 4).

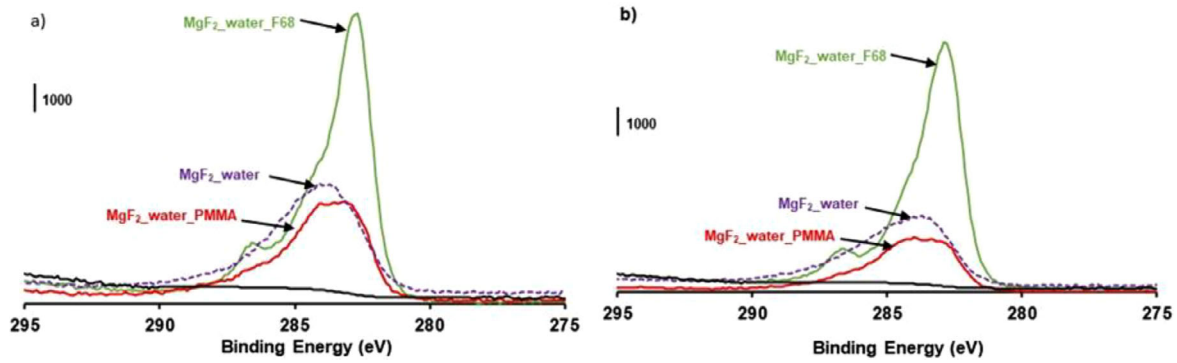

Figure 12. XPS spectra of the C 1s regions for MgF_2 prepared without polymer addition and with F68 or PMMA, a) before and b) after HF activation step.

Table 5. XPS analysis, atomic composition: Effect of the presence of a structuring agent during the synthesis of MgF_2 after activation by HF (350 °C, 1 h, N_2).

	Binding energy (eV) (atomic concentration (%))				Mg/F
	Mg 2s	F 1s	O1s	C 1s	
without structuring agent	89.9 (23)	684.8 (56)	531.5 (3)	283.7 (17)	0.41
F68	88.9 (17)	684.3 (41)	530.9 (6)	282.9 (37)	0.41
PMMA	89.4 (22)	684.9 (52)	531.6 (9)	284.0 (17)	0.42

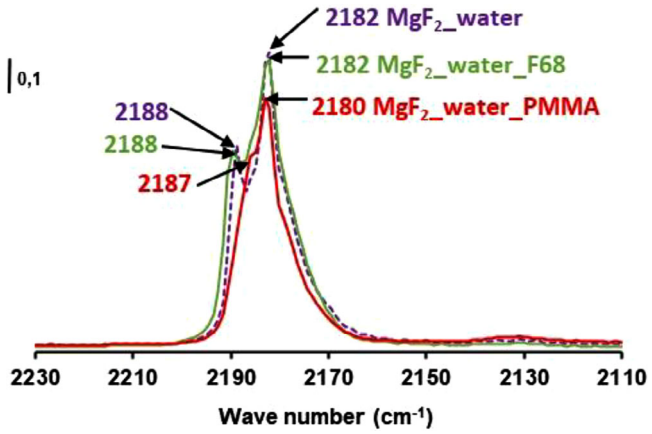

Figure 13. CO adsorption spectra: Influence of the presence of PMMA or F68 polymer, after HF activation step (350 °C, 1 h, N_2).

Table 6. Transformation of 2-chloropyridine. Influence of the use of microwaves (MW), the nature of solvent (water, methanol) and of the structuring agent (PMMA, F68) (T = 350 °C, HF/N_2/2ClPy = 6/1.7/1, isoconversion of 2chloropyridine (2ClPy) around 20%) (Activity (A): a) mmol h^{-1} g^{-1}, b) mmol h^{-1} m^{-2}, TOF: 'Turn Over Frequency, ($A_{/Qsites}$) h^{-1}, (Qsites: quantity of sites measured by FTIR-CO).

Sample	S_{BET} (m^2 g^{-1})	Activity		
		a)	b)	TOF
MgF_2_MW_methanol	49	32	0.65	400
MgF_2_methanol	39	40	1.00	82
MgF_2_water	47	40	0.85	70
MgF_2_water_PMMA	80	51	0.63	123
MgF_2_water_F68	69	52	0.75	100

3.2. Transformation of 2-Chloropyridine

A comparison of the preparation methods for bulk MgF_2 using microwave heating source (MW) or not and with methanol or water as solvent revealed no significant influence on catalytic activities for the transformation of 2-chloropyridine (Table 6). These activities were similar to those of the reference catalyst (MgF_2_MW_methanol) prepared in methanol with microwave heating (40 mmol·h^{-1}·g^{-1}). However, these values remain lower than the activity measured for MgF_2 prepared via the decomposition of magnesium trifluoroacetate (TFA route) (55 mmol·h^{-1}·g^{-1}).

When considering specific surface areas, all activities were lower than the calculated value for bulk MgF_2 prepared using the TFA method. For other samples, the activity was similar within experimental uncertainties. However, a notable increase in activity was observed when the MgF_2 bulk sample was prepared using PMMA or F68 as the structuring agent, in the absence of microwave heating and using water as solvent (MgF_2_water_PMMA). In this case, the catalytic activity (mmol$h^{-1}g^{-1}$) nearly doubled compared to MgF_2_MW_methanol and of 20% from MgF_2_water and very close to MgF_2 prepared via the TFA route. This improvement can be attributed, in part, to the increase in specific surface area (around 20%) from MgF_2_water. This leads to an activity per square meter very close (around 0.7). It also corresponds to a number of active sites and the strength of them close also. The turnover frequency (TOF), defined as the ratio of activity (A) to the number of active sites measured by FTIR-CO (Qsites), was found to vary slightly from 9.9 µmol.m^{-2} to 5.2, respectively, for MgF_2_water and MgF_2_water_PMMA. Specifically, the TOF increased from 70 h^{-1} for MgF_2_water to 100 h^{-1} MgF_2_water_PMMA as the spe-

cific surface area increased from 47 to 69 m^2g^{-1}. This observation highlights the critical importance of both the number and the intrinsic properties (strength) of the catalytic sites involved in the reaction. In contrast, only minor differences in the activity for the transformation of 2-chloropyridine were observed between the two polymers (PMMA and F68) under optimal conditions (no microwave heating and water as solvent). This indicates that the specific properties of PMMA and the surface-active properties of F68 are very close under these conditions. This interpretation is supported, on the one hand, by the identical rutile structure observed for the different MgF_2 samples, and on the other hand, by the XPS analysis of the surface of these samples, which was found to be identical. As a reminder, XPS is a technique that allows the analysis of the surface of a catalyst, corresponding to its catalytic surface. Conversely, polymer use appears to reduce aggregation, as TEM images reveal better-dispersed particles, resulting in increased specific surface area and potentially enhanced access to active sites. This is also consistent with the site concentration (C_sites), determined by FTIR-CO, which is lower in the presence of polymers (5.2 and 7.7 $\mu mol \cdot m^{-2}$ for MgF_2_water_PMMA and MgF_2_water_F68, respectively) compared to MgF_2_water (9.9 $\mu mol \cdot m^{-2}$). This decrease appears to favour the fluorination reaction by a better site accessibility through modifications in aggregate structuring, thereby affecting the distribution of sites on the surface of MgF_2 nanoparticles.

4. Conclusion

In this work, the optimization of various parameters involved in the synthesis of bulk MgF_2 was investigated. The best parameter is a synthesis in water and in the presence of a polymer (such as PMMA or Pluronic F68) in order to obtain the higher specific surface area under the operating conditions for measuring the catalytic performance of 2-chloropyridine, ($T = 350$ °C, in excess of HF). The rutile structure of MgF_2 remain unchanged and the specific surface area multiplied around by a factor two by the presence of a polymer during MgF_2 synthesis. This increase could be linked to a modification of the MgF_2 nanoparticle aggregates state. This key parameter leads to increase the catalytic activity for the transformation of 2-chloropyridine which is directly related to the higher specific surface areas. So, this investigation clearly shows the importance of the presence of a polymer during the synthesis of MgF_2 nanoparticles and this work could be extended by exploring other polymers in order to establish a relationship between the intrinsic properties of the polymers and the catalytic performances of the corresponding catalysts.

Acknowledgments

This work received funding from the French Agence Nationale de Recherche Project ANR-20-CE08-0026 "OPIFCat". A.I. The authors thank SYENSQO company (represented by Eric Périn and François Metz) and other colleagues in the OPIFCat project for useful scientific discussions. The Chevreul Institute is thanked for the XPS measurements of this work through the CHEMACT project supported by the "Ministère de l'Enseignement Supérieur et de la Recherche", the "CNRS", the region "Hauts-de-France" and the "Métropole Européenne de Lille".

Conflict of Interests

The authors declare no conflict of interest.

Data Availability Statement

The data that support the findings of this study are available from the corresponding author upon reasonable request.

Keywords: 2-Chloropyridine · Agglomerate · Hydrogen fluoride · Magnesium fluoride · Nanoparticle · Structuring agent

[1] J. Wang, M. Sánchez-Roselló, J. L. Aceña, C. Del Pozo, A. E. Sorochinsky, S. Fustero, V. A. Soloshonok, H. Liu, *Chem. Rev.* **2014**, *114*, 2432–2506.
[2] B. E. Smart, *J. Fluorine Chem.* **2001**, *109*, 3–11.
[3] M. Inoue, Y. Sumii, N. Shibata, *ACS Omega* **2020**, *5*, 10633–10640.
[4] L. Ruyet, "Synthèse douce et simple de molécules fluorées", https://www.inc.cnrs.fr/fr/cnrsinfo/synthese-douce-et-simple-de-molecules-fluorees.
[5] L. Ruyet, M. I. Lapuh, V. S. Koshti, T. Földesi, P. Jubault, T. Poisson, Z. Novák, T. Besset, *Chem. Commun.* **2021**, *57*, 6241–6244.
[6] E. Schmitt, B. Commare, A. Panossian, J.-P. Vors, S. Pazenok, F. R. Leroux, *Chem. - A Eur. J.* **2018**,*24*, 1311–1316.
[7] I. Davidson, R. Mcmillan, J. Murray, Z. Xin Shu, D. James Worsfold, WO9815024, **1998**.
[8] Y. Wang, W.-H. Zhong, A. Review", *ChemElectroChem* **2015**, *2*, 22–36.
[9] M. M. Thackeray, C. Wolverton, E. D. Isaacs, *Energy Environ. Sci.* **2012**, *5*, 7854.
[10] M. J. Molina, F. S. Rowland, *Nature* **1974**, *249*, 810–812.
[11] G. Balz, G. Schiemann, *Berichte Der Dtsch. Chem. Gesellschaft.* **1927**, *60*, 1186–1190.
[12] G. C. Finger, L. D. Starr, *J. Am. Chem. Soc.* **1959**, *81*, 2674–2675.
[13] G. C. Finger, L. D. Starr, D. R. Dickerson, H. S. Gutowsky, J. Hamer, *J. Org. Chem.* **1963**, *28*, 1666–1668.
[14] G. C. Finger, C. W. Kruse, *J. Am. Chem. Soc.* **1956**, *78*, 6034–6037.
[15] C. Cochon, T. Corre, S. Celerier, S. Brunet, *Appl. Catal. A Gen.* **2012**, *413–414*, 149–156.
[16] A. Astruc, C. Cochon, S. Dessources, S. Célérier, S. Brunet, *Appl. Catal. A Gen.* **2013**, *453* 20–27.
[17] Y. Wang, Z. Bajestani Gohari, J. Lhoste, S. Auguste, A. Hémon-Ribaud, M. Body, C. Legein, V. Maisonneuve, A. Guiet, S. Brunet, Z. Gohari Bajestani, J. Lhoste, S. Auguste, A. Hemon-Ribaud, M. Body, C. Legein, V. Maisonneuve, A. Guiet, S. Brunet, *Materials (Basel)* **2020**, *13* 3566.
[18] Z. Goharibajestani, Y. Wang, V. Camus-Génot, S. Arrii, J. D. Comparot, B. Polteau, J. Lhoste, C. Galven, V. Gunes, A. Hémon-Ribaud, S. Pascual, M. Body, C. Legein, V. Maisonneuve, S. Brunet, A. Guiet, *ACS Appl. Nano Mater.* **2021**, *4*, 10601–10612.
[19] E. Kemnitz, U. Groß, S. Rüdiger, C. S. Shekar, *Angew. Chemie - Int. Ed.* **2003**, *42*, 4251–4254.
[20] S. Rüdiger, G. Eltanany, U. Groß, E. Kemnitz, *J. Sol–Gel Sci. Technol.* **2007**, *41*, 299–311.
[21] R. König, G. Scholz, E. Kemnitz, *J. Sol–Gel Sci. Technol.* **2010**, *56*, 45–156.
[22] S. Wuttke, G. Scholz, S. Rüdiger, E. Kemnitz, *J. Mater. Chem.* **2007**,*17*, 4980.
[23] J. Krishna Murthy, U. Groß, S. Rüdiger, E. Kemnitz, J. M. Winfield, *J. Solid State Chem.* **2006**, *179*, 739–746.
[24] S. Wuttke, S. M. Coman, G. Scholz, H. Kirmse, A. Vimont, M. Daturi, S. L. M. Schroeder, E. Kemnitz, *Chem. - A Eur. J.* **2008**, *14*, 11488–11499.

[25] Y. Guo, S. Wuttke, A. Vimont, M. Daturi, J. C. Lavalley, K. Teinz, E. Kemnitz, *J. Mater. Chem.***2012**, *22*, 14587–14593.
[26] J. Krishna Murthy, U. Gross, S. Rüdiger, E. Kemnitz, *Appl. Catal. A Gen.* **2004**, *278*, 133–138.
[27] A. Demourgues, N. Penin, D. Dambournet, R. Clarenc, A. Tressaud, E. Durand, *J. Fluor. Chem.* **2012**, *134*, 35–43.
[28] M. Pietrowski, M. Wojciechowska, *J. Fluor. Chem.***2007**, *128*, 219–223.
[29] A. N. Arf, F. A. Kareem, S. S. Gul, *Polymers* **2023**, *15*, 1479.
[30] L. Toledo, D. Palacio, S. Sánchez, B. F. Urbano, *J. Mater. Sci.*,**2023**, *55*, 8968–8982.
[31] F. Rouquerol, J. Rouquerol, K. Sing, *In Adsorption by powders and porous solids, principle, Methodology and application*, Academic Press, London Second edition, **2014**.
[32] V. Camus-Genot, A. Guiet, J. Lhoste, F. Fayon, M. Body, S. Kodjikian, R. Moury, M. Leblanc, J.-L. Bobet, C. Legein, V. Maisonneuve, *Cryst. Growth Des.* **2021**, *21* 5914–5927.
[33] A. Impellizzeri, Dieu, J. R., S. Brunet, C. P. Ewels, *Catal. Sci. Technol.* **2024**, *14*, 3021–3028.

Manuscript received: June 30, 2025
Revised manuscript received: September 8, 2025
Accepted manuscript online: September 25, 2025
Version of record online: ■■, ■■